Theoretical Studies on the Potential Energy Surfaces of SO_2: Electronic States for Photodissociation from the $\tilde{C}^1B_2$ State

Kenshu KAMIYA*,† and Hiroyuki MATSUI
Department of Reaction Chemistry, The University of Tokyo, Hongo, Bunkyo-ku, Tokyo 113
(Received March 14, 1991)

The potential energy surfaces of electronically excited states of SO_2 have been investigated with ab initio molecular orbital method: Especially, the two-dimensional potential energy surface for the $\tilde{C}^1B_2$ ($2^1A'$) state as a function of both the bond angle and bond distance has been carefully analyzed, including the spin-orbit interaction. Energetically, $2^3A'$ (1^3A_1 in C_{2v}) was found to be the most probable state which concerns the reaction mechanism for the photodissociation pathway from the $\tilde{C}$ state (SO_2 ($\tilde{C}^1B_2$) $\rightarrow$ $SO(^3\Sigma^-)+O(^3P)$); however, other pathway may also be possible to go over the avoided crossing on a singlet potential surface.

Sulfur dioxide (SO_2) is well known as an important species concerning atmospheric chemistry and numerous studies have been carried out. Despite its importance, theoretical studies on SO_2, except for the ground state structure and properties, are relatively limited, especially regarding the structures of the potential energy surfaces in excited states.[1-5]

SO_2 is known to photodissociate under ultraviolet radiation at wavelengths shorter than about 220 nm;[6,7] and recent experimental studies using mainly the 193 nm line of an ArF laser have focused on its dissociation dynamics:[8-13] the photodissociation reaction has been recognized to be a predissociation from the $\tilde{C}^1B_2$ state producing the ground state product $SO(X^3\Sigma^-)$ and $O(^3P)$. The excited product ($SO(a^1\Delta)+O(^3P)$) has not been observed, even though it is energetically possible. Freedman et al.[8] first observed the time-of-flight spectrum of the dissociation product. Subsequently, the spectrum of the product SO has been measured by Kawasaki et al.[10] as well as by Felder et al.,[13] and the SO molecule has been found to be vibrationally excited with a maximum peak at $v=2$. Kanamori et al.[11] also observed a similar structure for both the vibrational and rotational distributions using a tunable diode laser. They also observed the spin polarization effect of the SO product, from which they concluded that most of the reaction proceeded via a triplet state. Moreover, they observed a minor peak of $SO(X^3\Sigma^-)$ at $v=5$, for which they suggested the mechanism via a singlet state. Ebata et al.[12] observed the rovibrational dependence of the predissociation rate and supported the mechanism via a triplet state.

In the present study we investigated the potential energy surfaces of SO_2 in excited states with ab initio CI method to clarify some aspects concerning SO_2 photochemistry, especially the possible photodissociation reaction pathways from the excited $\tilde{C}$ state and to the responsible electronic states for the reaction.

† Present address: School of Pharmaceutical Sciences, Kitasato University, Shirokane, Minato-ku, Tokyo 108.

Method

Potential energies were calculated using the configuration interaction (CI) method. Except for some preliminary search using the STO-3G basis set, the double zeta basis set augmented with polarization d-functions (DZP) were adopted for most of the calculations: the Dunning [4s, 2p][14] contraction of Huzinaga's (9s, 5p)[15] primitive set with a d-type function (exponent $\alpha=0.85$) was placed on oxygen, and the [6s, 4p][16] contraction of Huzinaga's (11s, 7p)[17] primitive set with a d-type function ($\alpha=0.6$) on sulfur. We also tried the extended basis set augmented with diffuse orbitals (DZP+d) in order to check the importance of Rydberg states. The molecular orbital sets used to construct CI expansion were calculated for the electronic ground state within the approximation of the restricted Hartree–Fock (RHF) theory and the improved virtual orbital (IVO)[18] technique. In order to refine the virtual orbitals using IVO, an electron was removed from the highest occupied $8a_1$ ($13a'$ in C_s structure) orbital to make a hole. For several calculations along the dissociation path of SO_2, the natural orbitals based on the unrestricted Hartree–Fock theory (UHFNO) were also used.

Two types of CI calculations were tried at the experimental equilibrium structure of the ground state.

1) V-SDTQ CI (valence- single, double, triple, and quadruple CI) with the DZP Basis Set: We considered all configurations up to 4 electron excitation from the ground-state configuration in the active space comprising of 10 valence orbitals (1s and 2sp orbitals of S and 1s and 2s of O were fixed as the core) with 14 electrons. The differences in energy spacing with the valence full CI, which included 6-electron excitation, were small. The numbers of configurations were between 729 and 1059 in C_{2v} symmetry.

2) MRSD CI (multi references single and double CI) with the Extended DZP+d Basis Set: s-, p-, and d-types of diffuse orbitals were placed on an S atom, and their exponents were optimized separately using RHF calculations for several Rydberg states. All of the virtual orbitals (except for several with extremely high energies) were considered to generate excitation configurations. For each spin and spatial symmetry in the C_{2v} point group, several tens of configurations were used as references; these were selected by considering preliminary small CI calculations. After perturbation selection with a 50 μhartree threshold in all of the single and double excitations from reference configurations, the dimensions of the matrices actually diagonalized were within

Table 1. The Vertical Excitation Energies at the Experimental Equilibrium Geometry of the Ground State of SO_2. The Energies in Unit of eV are Relative to 1^1A_1 State

State	MRSD CI (DZP+d)	V-SDTQ CI (DZP)	CI[a]	LDF[b]
Singlet:				
1^1A_1	0.00	0.00	0.00	0.0
1^1B_1	4.34	4.67	3.70	3.9
1^1A_2	4.47	5.00	4.77	5.0
1^1B_2	6.75	6.82	6.93	5.9
2^1A_1	9.08	8.98		
2^1B_1	8.84	8.73		
3^1A_1	9.56	9.66		
2^1A_2	9.10	8.77		
Triplet:				
1^3B_1	3.74	3.67	2.52	3.2
1^3B_2	4.23	4.60	2.54	4.8
1^3A_2	4.45	4.86		
1^3A_1	7.81	7.82	4.21	4.6
2^3B_2	8.87	9.28		
2^3B_1	8.37	8.37		
2^3A_1	10.22	9.07		
2^3A_2	9.08	8.55		

a) Single excitation CI within 6 valence orbitals using 4-31G basis set (Ref. 3). b) The local density functional calculation (Ref. 1).

the range from 3000 to 15000.

The second MRSD CI calculations were mainly intended to test the reliability of more tractable V-SDTQ CI calculations. After a comparison of the two types of calculations (Table 1), we found that the order in energy of the important low-lying states was identical in these two types of calculations, although the differences of the energy levels were several tenths of an eV. Despite the differences in energy, the results with V-SDTQ CI were used in this study for qualitative discussions concerning the reaction mechanism. In the MRSD CI calculations, Rydberg states did not appear in the region less than 10 eV, indicating a minor importance of such states in photochemical events concerning the $\tilde{C}$ state. Thus, most of the calculations were carried out with V-SDTQ CI using the DZP basis set without diffuse orbitals.

Results

1. The Equilibrium Structures and Energies. The optimum structures for the ground state $\tilde{X}^1A_1$ and the singlet excited state $\tilde{C}^1B_2(2^1A')$ were searched for using the V-SDTQ CI calculation. The excited $\tilde{C}$ state has been known to have an asymmetric structure.[19] The bond distance and angle for the ground state for the optimized structure in this calculation are R=2.775 Bohr (1.468 Å) and θ=122 degrees, respectively; they roughly agree with experimentally determined values, R=2.706 (1.432 Å) and θ=119.5.[20] Those for the $\tilde{C}$ state are R_1=2.869 Bohr (1.518 Å), R_2=3.467 Bohr (1.835 Å) and θ=108.3 degrees (experimental values are: R_1=2.818 (1.491 Å), R_2=3.097 (1.639 Å) and θ=103.75[19]). The adiabatic excitation energy, $\tilde{C}^1A'\leftarrow\tilde{X}^1A_1$, without a zero-point energy correction was calculated to be 5.00 eV, while the experimental value with zero-point energy is 5.28 eV.[19]

2. Angular Dependence of the Potential Energy. Figure 2 shows the potential energy surfaces of each electronic state as functions of the bond angle calculated in this study. Qualitatively, the shapes of the potential curves and the features of crossings are in good agreement with other theoretical results (SCF[4] or the local density functional theory[1]) although small discrepancies have been found, which may be partly due to differences in the geometries. We will discuss the features on each electronic state separately.

^{1}A′ States ($^1A_1$, $^1B_2$). The electronic configuration of the ground state is (see Fig. 1)

$\tilde{X}^1A_1$:……$(2b_1)^2(5b_2)^2(1a_2)^2(8a_1)^2$.

$\tilde{C}^1B_2(1a_2\rightarrow 3b_1)$ is the second singlet A′ state when its geometry is close to the equilibrium structure of the ground state. The state which is usually denoted 2^1A_1 shows a minimum at the angular region 40—60 degrees, and comprises the electronic state $(5b_2)^2\rightarrow(3b_1)^2$, which has 6 electrons in out-of-plane π orbitals. The corresponding state of O_3 is known to have a ring structure(D_{3h}). This state rapidly increases in energy as the angle becomes larger, and then crosses with $\tilde{X}^1A_1$. We did not attempt more detailed calculations for the coupling of the two states ($\tilde{X}^1A_1$ and 2^1A_1). At nearly 70 degrees, the state (2^1A_1), which no longer has the ring state character, crosses with 1^1B_2. Above 120 degrees the energy of 2^1A_1, whose dominant configuration is now $8a_1\rightarrow 9a_1$, decreases as the angle increases; the state crosses again with 1^1B_2 at nearly 145 degrees, and correlates adiabatically to $^1\Pi_u$ at 180 degrees, degenerating with 1^1B_1 state.

There seems to be no large contamination of the 1^1A_1 and 1^1B_2 states. In the equilibrium structure, 1^1A_1 has 6 electrons in the in-plane π orbitals (n orbitals) and 4 electrons in the out-of-plane π orbitals. This electronic configuration might be expected to correlate to a Δ state when in a linear structure as the in-plane and out-of-plane π orbitals degenerate, as reported for the O_3 molecule. In fact, the ground state correlates to the $^1\Sigma_g^+$ state when in a linear structure. We will discuss the electronic states later. The 1^1B_2 state degenerates with 2^1A_2 and correlates to $^1\Delta$.

^{1,3}A″ (B_1, A_2) State. The shapes of the potential curves are almost parallel to the corresponding singlet and triplet states, and the triplet states are slightly lower in energy than the singlets. For both spin states, the potential surfaces of the first B_1 ($8a_1\rightarrow 3b_1$) and the first A_2 ($5b_2\rightarrow 3b_1$) closely approach; the minimum of the former is at ca. 125 degrees, and that for the latter is at ca. 100 degrees, consequently giving a conical crossing between them. The $^1B_1$ and $^3B_1$ states degenerate when in a linear structure with 2^1A_1 and 1^3A_1, respectively, and correlate to Π_u states.

^{3}A′ State ($^3A_1$, $^3B_2$). Similarly to the case of A″, the

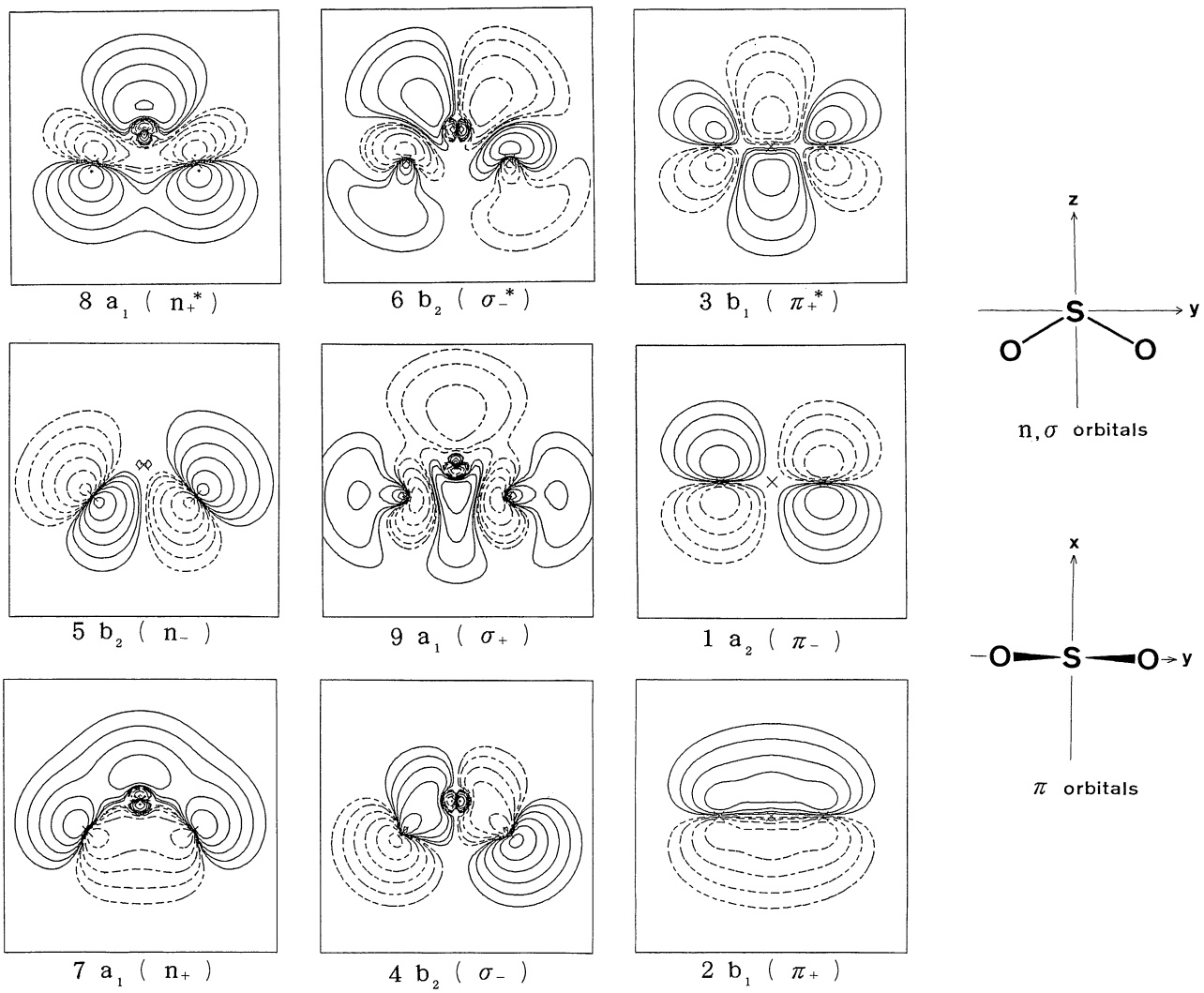

Fig. 1. The typical valence orbitals calculated with RHF/DZP for the ground state at the experimental equilibrium structure. Contour maps are drawn at the intersections with YZ- and XY-planes for n, σ, and π orbitals, respectively.

potential curves of the lower electronic states (1^3A_1 and 1^3B_2) have similar shapes as those of the corresponding singlet states (2^1A_1 and 1^1B_2). At nearly 150 degrees 1^3A_1 and 1^3B_2 cross, just as for the singlet states. 1^3A_1 correlates to $^3\Pi_u$, and degenerates with 1^3B_1.

3. Electronic States at Linear Structure. As shown in Fig. 2, the ground and low-lying excited states have energy minima with the bond angles of 90—130 degrees, except for 1^3A_1 and 2^1A_1, which are both Renner–Teller coupling pairs with 1^3B_1 and 1^1B_1, respectively. In order to resolve spectroscopic problems and photochemical processes, it is important to investigate the electronic states in a linear structure.

As described above, the electronic ground state 1^1A_1 correlates to $^1\Sigma_g^+$ in a linear structure, not $^1\Delta_g$, a degenerate state, which is reported to be the case for O_3.[21] It is 2^1A_1 that degenerates with 1^1B_1 and correlates to the $^1\Pi_u$ state. The reason why the ground state does not degenerate when in a linear structure is that the highest occupied $8a_1$ orbital (a π orbital in the molecular plane (n_+*)) couples with the $9a_1$ orbital and adiabatically correlates to σ_g^+ of a linear molecule.

Table 2 shows the energies for linear structures of O_3 and SO_2 in several electronic states, calculated with the open-shell restricted Hartree–Fock approximation. Two electrons occupying three orbitals (π_u and σ_g^+, noted above) make six independent electronic states corresponding to three electronic configurations: $(\pi_u)^2$, $(\pi_u)^1(\sigma_g)^1$, $(\sigma_g)^2$. ($^1\Delta_g$, $^3\Sigma_g^-$, $^1\Sigma_g^+$ states are from $(\pi_u)^2$, $^1\Pi_u$, $^3\Pi_u$ from $(\pi_u)^1(\sigma_g)^1$, and another $^1\Sigma_g^+$ from $(\sigma_g)^2$.) For both SO_2 and O_3, the orders in energies of the three states within $(\pi_u)^2$ and the two states within $(\pi_u)^1(\sigma_g)^1$ obey Hund's rule. The energies of the three configurations, however, were reverse in order for SO_2 and O_3 with the DZP basis set. This may reflect the difference in the order of the two orbitals, σ_g and π_u, for SO_2 and O_3. The

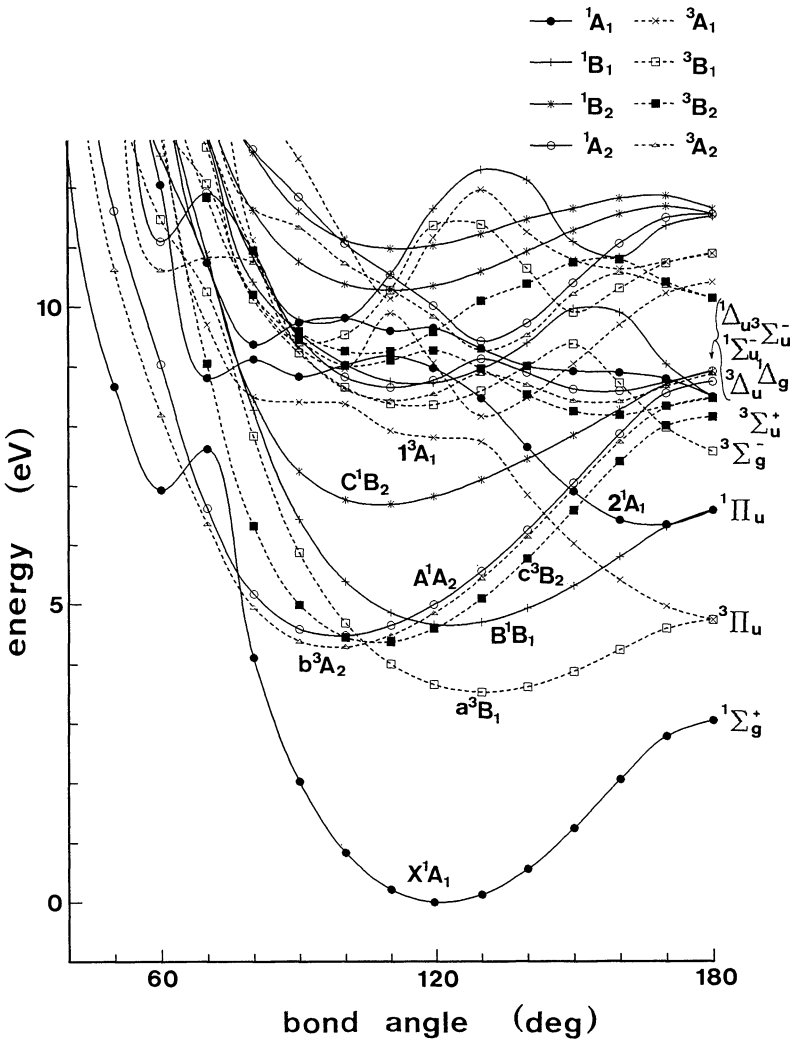

Fig. 2. The potential energies of the low lying states of SO_2 as a function of bond angle at R=2.706 Bohr (experimental equilibrium S–O distance for the ground state).

Table 2. The Energies of the Lower Electronic States of O_3 and SO_2 at Liner ($D_{\infty h}$) Structures with Experimental Bond Distances (R=2.415 Bohr (O_3), 2.7063 Bohr (SO_2)) Calculated with RHF, Units are in Hartree

State	O_3		SO_2		
	STO-3G	DZP	STO-3G	DZP	CI (DZP)
$(\pi_u)^2$					
$^3\Sigma_g^-$	−221.25460	−224.25073	−540.45524	−546.94084	−547.00815
$^1\Delta_g$	−221.21436	−224.21070	−540.42021	−546.90707	−546.97463
$^1\Sigma_g^+$	−221.17491	−224.17337	−540.38547	−546.87446	—
$(\pi_u)^1(\sigma_g)^1$					
$^3\Pi_u$	−221.04974	−224.08786	−540.40869	−547.03197	−547.11253
$^1\Pi_u$	−220.98886	−224.02859	−540.34796	−546.94870	−547.04467
$(\sigma_g)^2$					
$^1\Sigma_g^+$	−220.77410	−223.86546	−540.29289	−547.05265	−547.17483

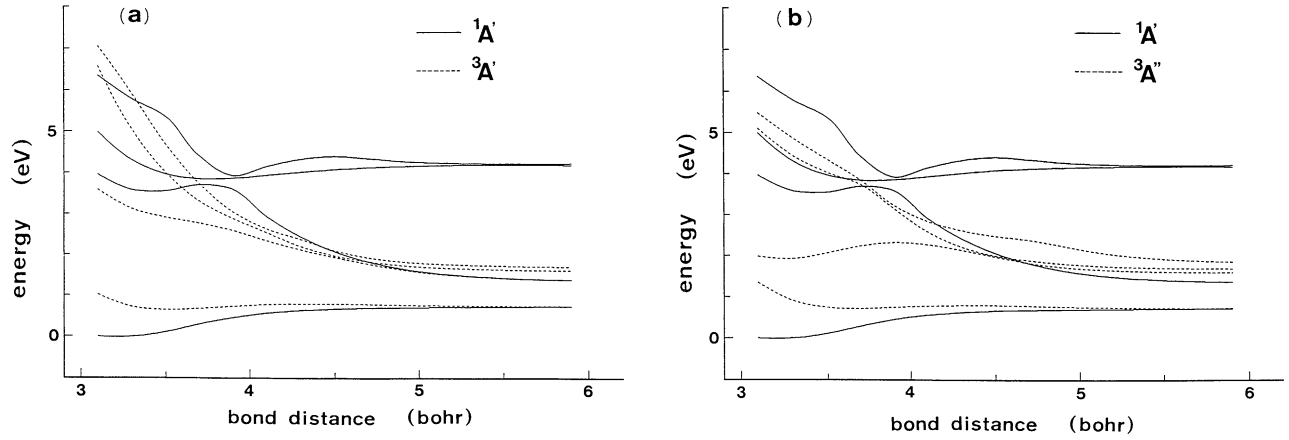

Fig. 3. The potential energy curves along the path $SO_2 \rightarrow SO+O$ as a function of the dissociative bond distance. The other bond distance and bond angle are fixed. (a) $^1A'$–$^3A'$, (b) $^1A'$–$^3A''$. (STO-3G, V-SDTQ CI).

effect of basis sets was important for calculating the order of the states in SO_2. The results with STO-3G showed a reverse order from those with DZP, while the two basis sets gave the same results for O_3.

A mechanism based on a Renner–Teller coupling of $^1A_1$ and $^1B_1$ into $^1\Delta_g$ for the ground state has been postulated[22] in order to interpret the UV absorption of SO_2 in the range from 340 to 250 nm. However the present calculation shows that the state from the Renner–Teller coupling of 2^1A_1 and 1^1B_1 is $^1\Pi_u(\sigma_g^+ \rightarrow \pi_u)$, and not the ground state, $^1A_1$.

We also checked the energy changes of each state with an asymmetric deformation. Calculations were performed while constraining one SO bond to be fixed, with the bond angle at 180 degrees. While most of the states were unstable and/or dissociative under such an asymmetric deformation, the potential curve of the ground state and the lowest triplet state, $^3\Pi_u$, showed a minimum at the point where the two SO bond distances were the same. The $^3\Pi_u$ was the only state which was lower in energy when in a $D_{\infty h}$ structure than the dissociation energy of the ground states. The $^3\Pi_u$ caused a Renner–Teller splitting under a deformation of the bond angle (as noted above), and the upper state of the pair, $^3A_1$, showed a minimum when in the $D_{\infty h}$ structure. The corresponding singlet Renner–Teller state, $^1\Pi_u$, was higher in energy than the dissociation limit of the ground state, and the upper state $^1A_1$ at $D_{\infty h}$ structure was unstable regarding both a deformation of the bond angle and the bond distance.

4. Potential Energies along the Dissociation $SO_2 \rightarrow SO+O$. In order to discuss the qualitative features of the potential energy surfaces along its dissociation path, some results of preliminary calculations using the STO-3G, V-SDTQ CI based on UHF natural orbitals are shown in Fig. 3. The UHF orbitals can approximately connect the electronic states continuously to the dissociation limit. Note that the calculated energies using STO-3G are less reliable than those using DZP basis sets. All of the degrees of freedom of the molecule were fixed to the experimental equilibrium structure of the $\tilde{C}$ state, except for the dissociative SO bond length, which was varied over a wide range. The lowest four states for each symmetry of $^1A'$, $^3A'$, and $^3A''$ are shown in this figure in order to demonstrate the relationship between the $\tilde{C}$ state and the

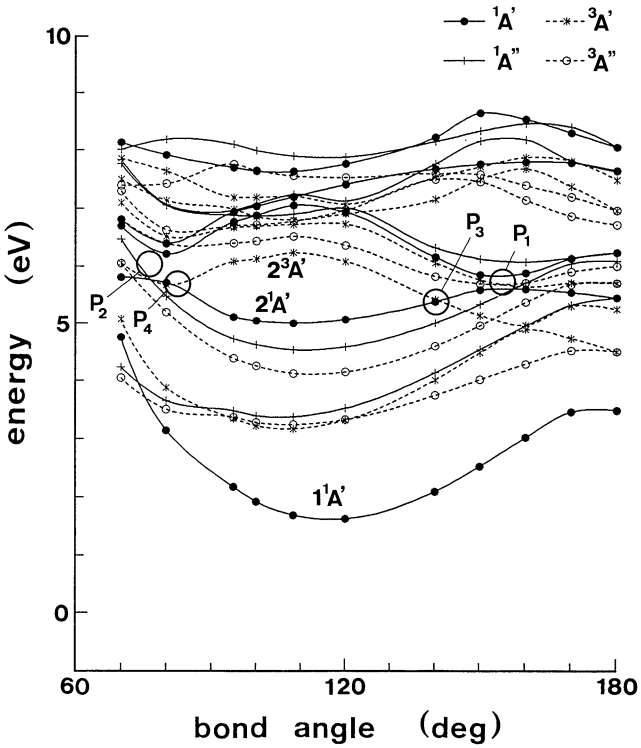

Fig. 4. The potential energies of the low lying states of SO_2 as a function of bond angle at (R_1, R_2)=(2.869 Bohr, 3.467 Bohr) (calculated equilibrium S–O distances for the $\tilde{C}$ state). Zero of energy is for the equilibrium of the ground state. Symbols P_1—P_4 are the crossing points between the $\tilde{C}$ state and $3^1A'$ or $2^3A'$ states.

other triplet states. As shown in the figures, the second $^1A'$ state (corresponds to the $\tilde{C}$ state) correlates to the excited state of products $SO(^1\Sigma^-)+O(^1D)$. The state encounters crossings and/or avoided crossings with another state which correlates to the excited-state product or with the repulsive state which correlates to the ground-state product. It should be noted that a similar structure to that of the singlet surfaces is found in the O_3 system.[23] The $\tilde{C}$ state crosses with several triplet states: 2-4$^3A'$ and 3,4$^3A''$. Although the crossing between $2^1A'$ and $2^3A'$ is not shown in the figure, the crossing appeared in more sophisticated calculations using the DZP basis set.

5. Potential Energy Surface of the Photodissociation from the $\tilde{C}$ State. As noted above, the potential energy surface of the $\tilde{C}^1B_2$ state crosses with another repulsive singlet state and with several triplet states as one of the bond distances is changed. It also crosses with the $^1A_1$ and $^3A_1$ states as the bond angle is changed. In order to examine the features of the potential energy surface crossings, we calculated the potential surfaces as a function of two parameters (one SO bond length (R) and the bond angle (θ)) with the other SO bond length fixed to 2.869 Bohr (the calculated equilibrium bond distance of the shorter SO bond of the $\tilde{C}$ state). Such constraint seems adequate for a qualitative description of the reaction system, since the bond distance of the dissociation product, $SO(^3\Sigma^-)$, calculated to be 2.909 Bohr, was not much different from that of the shorter SO bond of the equilibrium structure of the $\tilde{C}$ state.

Figure 4 shows the cross section of the potential surfaces at R=3.467 Bohr, the calculated equilibrium distance of the longer SO bond of the $\tilde{C}^1A'$ state. Although we do not show any detailed assignments for the uppper states, one can recognize the manifold of the electronic states above 6 eV from the equilibrium of the ground state. The potential curves of the $\tilde{C}^1A'$ and $3^1A'$ states (1^1B_2 and 2^1A_1 in C_{2v} structure, respectively) cross at two points (P_1 and P_2), as shown in the figure. Although the crossing should be avoided, since the two states belong to the same symmetry A' in the C_s point group, the coupling of the states was found to be weak. At crossing point P_1, which is placed at a larger bond angle and lower in energy, the dominant configurations of $2^1A'(\tilde{C}$ state) and $3^1A'$ are $\pi_-\rightarrow\pi_+^*$ and $n_+^*\rightarrow\sigma_+$, respectively. As the bond distance (R) becomes larger, the two states become strongly mixed to give a larger separation. The state which corresponds to $n_+^*\rightarrow\sigma_+$ degenerates with $1^1A''$ (1^1B_1 in C_{2v}) when in a linear

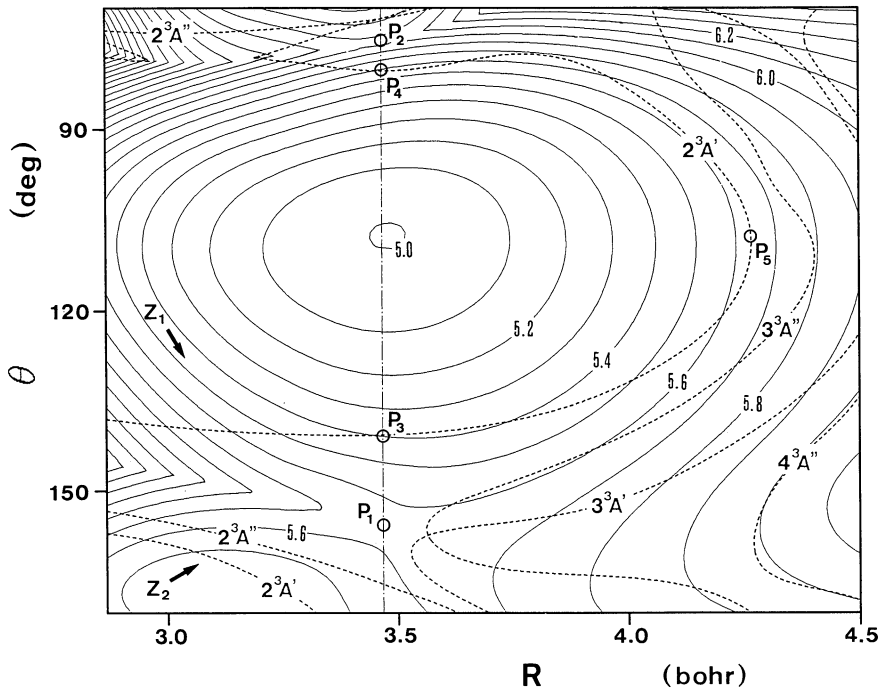

Fig. 5. The potential energy of the $\tilde{C}(2^1A')$ state as a function of the bond angle θ and one of the bond distances R with another bond distance being fixed to 2.869 Bohr. The contour energies are in eV (relative energy from the calculated ground state at equilibrium). The dashed curves are crossing seams with the triplet states ($2^3A'$, $3^3A'$, $2^3A''$, $3^3A''$, and $4^3A''$). Symbols P_3, P_4, and P_5 are the points on the crossing seams between $2^1A'$ and $2^3A'$ where magnitude of the transition probabilities were estimated (see text). The dash-dot line corresponds to the position of the cross section shown in Fig. 4. The arrows Z_1 and Z_2 are shown to indicate the approximate direction of view for (1) and (2) of Fig. 6, respectively.

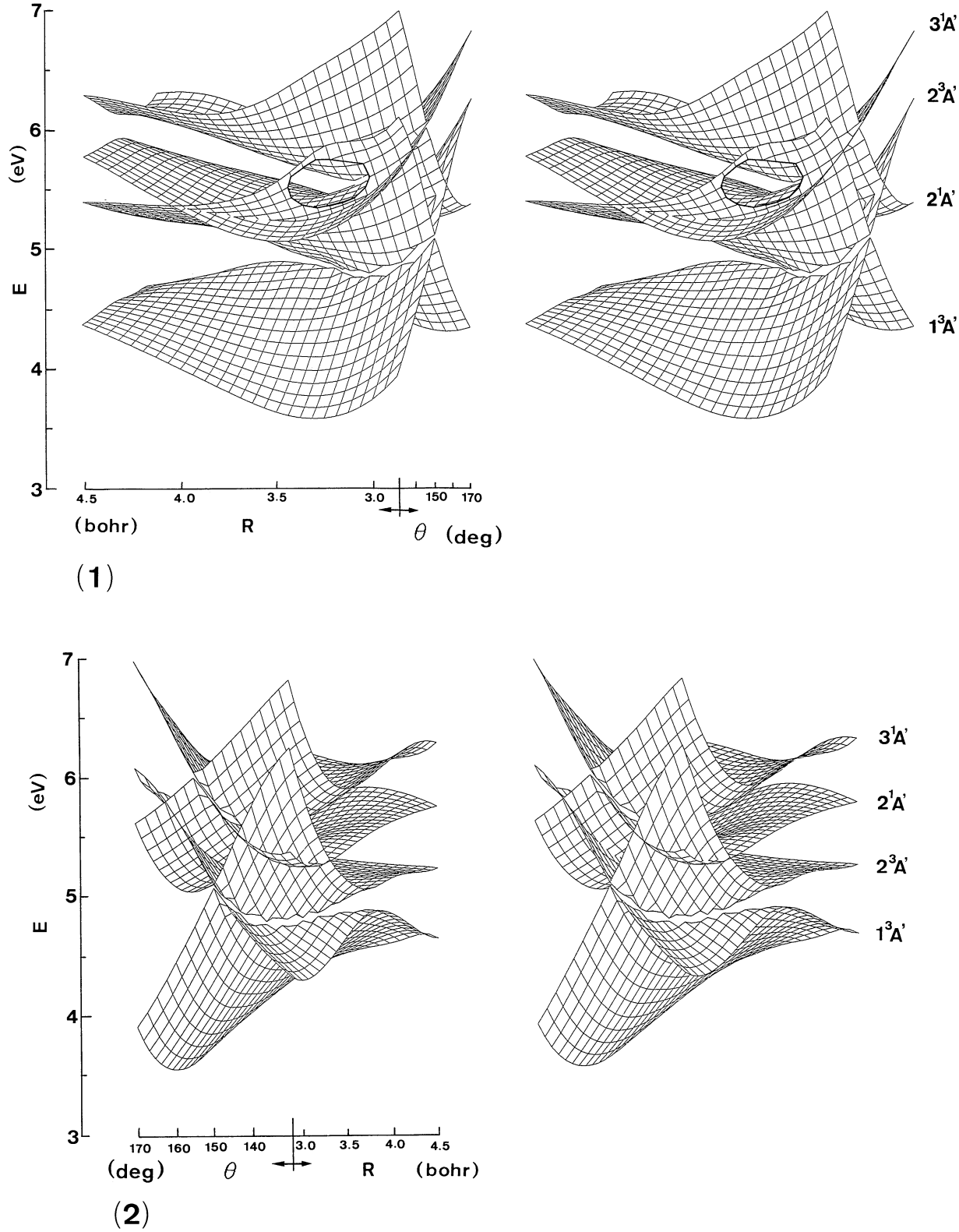

Fig. 6. Stereoscopic view of the potential energy surfaces at the region of crossing or avoided crossing including $2^1A'$ ($\tilde{C}$), $3^1A'$, $1^3A'$, and $2^3A'$ states. The potential surfaces within rectangular region (θ=130—170 degree and R=2.875—4.500 Bohr) are shown, and each approximate directions of view for (1) and (2) are shown in Fig. 5 by the arrows Z_1 and Z_2, respectively. A part of the $2^3A'$ surface in (1) is cut off to show the saddle point on the $2^1A'$ surface.

structure, giving $^1\Pi$, which correlates to the ground state of the product at infinite R.

Figure 4 also shows the crossing points between the $\tilde{C}$ state and $2^3A'(1^3A_1$ in $C_{2v})$: P_3 and P_4. They are slightly lower in energy than those between the $\tilde{C}$ state and $3^1A'$. This reflects that $2^3A'$ is lower in energy than $3^1A'$, originating from a difference in the exchange interaction of each spin state.

Figure 5 shows a potential map of the $\tilde{C}$ state as a function of R and θ. It is drawn adiabatically along the second root of CI for the $^1A'$ states. The dashed curves in the figure indicate the seams of the crossing between the $\tilde{C}$ state and other triplet states; P_3, P_4 (already shown in Fig. 4) and P_5 are the representative points on the crossing between the $\tilde{C}$ state and $2^3A'$ (discussed later). At θ=150—160 degrees, there exists a saddle due to the avoided crossing with the $3^1A'$ state. Also shown in the figure are the several triplet states crossing with the $\tilde{C}$ state surface at regions which are lower in energy than the singlet saddle point. Of these triplets, $2^3A'$ (1^3A_1 in C_{2v}), whose crossing is the lowest, is the only state to correlate to the ground-state product. Note that both the saddle point on the singlet surface and the minimum point on the crossing seam with $2^3A'$ are placed at a region of larger angle θ that the minimum of the potential.

Figure 6 shows schemata of the potential energy surfaces as functions of R and θ at the avoided crossing region of $2^1A'$ and $3^1A'$ (upper two surfaces in the figure), which is mentioned above. Although the energy spacing of the avoided crossing between the two states is not accurate, the avoided crossing region corresponds to that of the saddle point of the $^1A'$ surface. The saddle on the singlet surface is the lowest point on the crossing seam and corresponds to the possible transition point of the dissociation reaction from the $\tilde{C}$ state to the ground-state product if the reaction proceeds on a singlet adiabatic potential surface. The $2^3A'$ and $1^3A'$ states are also shown in the figure (lower two surfaces) in order to show the features of the crossings and the minimum crossing point of the $2^3A'$ and $\tilde{C}$ states. The two triplet states show crossing or avoided crossing features similar to those of the singlets, originating from the same dominant configurations, except for the spin states. The $2^3A'$ (1^3A_1 in C_{2v}) state crosses with $\tilde{C}^3B_2$ in C_{2v} symmetry and correlates to the lowest triplet state, $^3\Pi_u$, which has a minimum when in a linear structure. Although the crossing should be avoided with asymmetric deformation, both of the triplet states correlate to the ground-state product when R is infinity.

Discussion on the Reaction Pathways of the Photodissociation from the $\tilde{C}$ State

One of the experimental findings concerning the UV photodissociation on O_3 is that the excitation of the antisymmetric stretching mode enhances the reaction from the $\tilde{C}$ state.[24] SO_2 has also been reported to show a similar trend, that the excitation of the antisymmetric mode is important rather than the bending mode.[25] Because of the difference in the equilibrium structures of the ground state and the $\tilde{C}$ state, the electronically excited SO_2 is also vibrationally excited. The molecule is also expected to experience considerable vibrations within its longer lifetime than the rotational period before its predissociation.[9]

Based on our calculated results, we can discuss the highest energy point (transition state) along the minimum-energy path from the minimum of the $\tilde{C}$ state to the product ground state. If we assume that the reaction proceeds on a singlet adiabatic surface (called the singlet mechanism), the transition state should be a saddle on the barrier arising from the avoided crossing between $\tilde{C}$ state and $3^1A'$ (2^1A_1 in C_{2v}, $1^1\Pi_u$ in $D_{\infty h}$). In contrast, if the reaction is allowed one singlet-triplet transition (namely, the triplet mechanism), the most probable transition state (the lowest in energy and not requiring further crossing to reach ground state product) is the minimum point on the crossing seam between the $\tilde{C}$ states and the $2^3A'$ (1^3A_1 in C_{2v}, $1^3\Pi_u$ in $D_{\infty h}$) state. As described above, the triplet transition point was lower in energy: thus, the triplet mechanism may be advantageous from an energetical point of view. However, both transition points are placed at the larger bond-angle side of the minimum of the $\tilde{C}$ state. Thid seems to contradict the experimental result that the bending vibration is not important. However, the following comments and discussions may be possible, especially regarding the triplet mechanism.

The photon energy of the ArF laser (193 nm, 6.42 eV) is about 1.1 eV higher than the minimum energy of the $\tilde{C}$ state. According to our results, for the singlet mechanism the saddle point region is the only exit to the dissociation product with a threshold energy of 1.1 eV, meaning that bending motion is necessary for the reaction. For the triplet mechanism, however, the singlet–triplet crossing seams are located over a wide region on the surfaces, which is energetically accessible, including the larger bond distance side of the minimum of the $\tilde{C}$ state. Moreover, the crossing seam runs nearly parallel to the equipotential curves of the singlet surface, meaning that the energy change along the seam is not very drastic. That is, the singlet–triplet transition may not be so concentrated only near the minimum transition point.

It may be possible to roughly estimate the transition probabilities from the potential and the wave function. We estimated the matrix elements for a singlet–triplet spin orbit interaction in the following semiempirical way. In the usual spin orbit coupling Hamiltonian, the second term (spin-other-orbit-interaction) was neglected:

$$H_{so}=\frac{\alpha^2}{2}\sum_i\sum_A\frac{Z_A}{r_{iA}^3}(\boldsymbol{l}_{iA}\cdot\boldsymbol{s}_i)-\frac{\alpha^2}{2}\sum_{i,j}\left(\frac{\boldsymbol{r}_{ij}}{r_{ij}^3}\times\boldsymbol{p}_i\right)\cdot(\boldsymbol{s}_i+2\boldsymbol{s}_j). \quad (1)$$

Further, the multi-center integrals in the first term were neglected, and the effective nuclear charges (Z_A) were

Table 3. The Amount of the Transition Probability F between $2^1A'$ ($\tilde{C}$ State) and $2^3A'$ at the Point near the Crossing Seam between the States. One of the SO Bond is Fixed at 2.869 au

	Geometry (R/au	θ/deg)	Energy[a]/au	$\|G\|/10^{-4}$ au	$V^2/10^{-8}$ au	F[b]
P_3:	(3.467	140.0)	0.01472	3.812	6.1898	1
P_4:	(3.467	80.0)	0.02556	8.314	5.4402	0.40
P_5:	(4.250	108.3)	0.02274	3.362	9.9128	1.85

a) Mean values of the single and the triplet, relative to the minimum of $\tilde{C}(2^1A')$. b) Relative value to the point P_3.

treated as being adjustable parameters and were determined so as to fit the fine structures of the atomic spectrum. We adopted values of $Z_{sulfur}=13.698$ and $Z_{oxygen}=5.304$ using the results of SCF calculations for S and O atoms. If we consider that the velocity component which is perpendicular to the singlet-triplet crossing, determines the transition, the Landau–Zener transition probability can be expressed as follows:

$$\chi(\boldsymbol{p},\boldsymbol{q})=1-\exp(-\zeta), \tag{2}$$

where

$$\zeta=\frac{2\pi V(\boldsymbol{q})^2}{\hbar v|\boldsymbol{G}(\boldsymbol{q})|}.$$

Here, $V(\boldsymbol{q})$ denotes the absolute value of the elecronic singlet–triplet coupling, $|\langle S|H_{el}|T\rangle|$, and $\boldsymbol{G}(\boldsymbol{q})$ denotes the difference in the gradients of the singlet and triplet,

$$\boldsymbol{G}(\boldsymbol{q})=\frac{d}{d\boldsymbol{q}}({}^1E(\boldsymbol{q})-{}^3E(\boldsymbol{q})).$$

Further, v represents the velocity component perpendicular to the crossing seam

$$v=\frac{\boldsymbol{p}\cdot\boldsymbol{G}(\boldsymbol{q})}{m|\boldsymbol{G}(\boldsymbol{q})|}.$$

Here, we define $F(\boldsymbol{q})$ as being a factor which is not dependent on velocity,

$$F(\boldsymbol{q})=\frac{V(\boldsymbol{q})^2}{|\boldsymbol{G}(\boldsymbol{q})|}. \tag{3}$$

$F(\boldsymbol{q})$ can be considered to be a simple index which shows the reference value of the amount of the transition probability.

The F value was calculated at the points P_3, P_4, and P_5 on the two-dimensional potential surface of Fig. 5. P_3 and P_4 are the points where the normal of the seam corresponds to the bending (larger and smaller side of the minimum, respectively), and P_5 the point where the normal corresponds to antisymmetric stretching. As shown in Table 3, F at P_5 was 1.8-times larger than at P_3. It is thus possible that point P_5 is more important than point P_3, although the energy of the former is 8 m hartree (0.22 eV) higher than the latter.

It is apparent, however, the present calculation does not have sufficient quality to discuss further either the energetics or the quality of the wave functions, as one can find after a comparison with the larger CI calculations given in Table 1. Ebata et al.[12] observed the threshold energy of the predissociation to be about 0.35 eV higher than E_0 of the $\tilde{C}$ state; the zero point energy is about 0.1 eV. The calculated energies of points P_3 and P_5 are 0.40 and 0.62 eV higher than the minimum of the $\tilde{C}$ state, respectively. Considering that the structures of the crossing points are not fully optimized, the discussion given above is only qualitatively meaningful.

The effect of the other bond length, which was frozen at the fixed value throughout this study, may also be significant. Although the bond distances of the shorter bond of the molecule in the $\tilde{C}$ state is similar to that of the product, SO, it may be possible that the shorter bond of SO_2 is also vibrationally excited by 193 nm excitation; such an effect can be important in producing a vibrationally excited product, SO, as was observed in some experiments.

Another mechanism may be possible to interpret the minor importance of the bending mode. The bending vibration may cause multiple crossing of the seams while antisymmetric stretching motion is directly connected to dissociative motion. There is no potential structure to enhance the dissociation after the singlet–triplet transition with bending motion, since the $^3\Pi_u$ state is a bound state and has a minimum when in a linear structure.

There exist some experimental evidence that most of the reaction proceeds via a triplet state.[9-12] We have shown the advantage of the triplet mechanism regarding energy, although it is not conclusive because of difficulties in comparing the two different mechanisms.

Kanamori et al.[11] observed two types of product SO fragments; the major one, which had vibrational quantum numbers $v=1$ and $v=2$, showed a spin polarization effect; the minor one, which was in $v=5$, did not. They suggested that this result is a combination of two mechanisms: the major is via a triplet and the minor via a singlet; the possibility of the two pathways, which we suggest here, may correspond to those of Kanamori's results.

Conlcusion

The excited state potential energy surface of SO_2 was calculated using the CI method. The angular dependence of the energy level of each state was presented, showing a qualitatively similar structure as that in previous theoretical calculations.

The structure of the potential energy surfaces and their crossing with the $\tilde{C}$ state were examined in order to obtain insight into the UV photodissociation mechanism and to identify the responsible electronic states for the reaction. It was found that several triplet states did cross with the $\tilde{C}$ state in an energetically accessible region. The most probable state was $2^3A'$ (1^3A_1 in C_{2v}, $^3\Pi_u$ in $D_{\infty h}$), which became the upper state of the Renner–Teller coupling pair when in a nearly linear structure, and had an equilibrium structure with a $D_{\infty h}$ symmetry. The reaction path on the singlet adiabatic surface was also energetically possible through the avoided crossing between the $\tilde{C}$ state and other singlet excited state (2^1A_1 in C_{2v}, $1^1\Pi_u$ in $D_{\infty h}$), but energetically less favorable than the triplet mechanism.

However, the results suggested by the present work should be accepted only qualitatively. We could not give any conclusive discussion concerning the two kind of possible pathways, the singlet and the triplet mechanisms. More quantitative and sophisticated calculations are necessary for any further discussion.

The authors gratefully acknowledge to Professor K. Morokuma (Institute for Molecular Science) and Professor E. R. Davidson (Indiana University) for thier guidance and helpful discussions. All the numerical calculations were carried out at the Computer Center of Institute for Molecular Science using the program MELD.[26]

References

1) R. O. Jones, *J. Chem. Phys.*, **82**, 325 (1985).
2) I. H. Hillier and V. R. Saunders, *Mol. Phys.*, **22**, 193 (1971).
3) G. L. Bendazzoli and P. Palmieri, *Int. J. Quantum Chem.*, **9**, 537 (1975).
4) R. J. Zellmer, Master's Thesis, Department of Chemistry, The Ohio State University, Columbus, Ohio (1981).
5) P. Phillips and E. R. Davidson, *J. Comput. Chem.*, **4**, 337 (1983).
6) H. Okabe, *J. Am. Chem. Soc.*, **93**, 7095 (1971).
7) M. H. Hui and S. A. Rice, *Chem. Phys. Lett.*, **17**, 474 (1972).
8) A. Freedman, S. C. Yang, and R. Bersohn, *J. Chem. Phys.*, **70**, 5313 (1979).
9) M. Kawasaki, K. Kasatani, H. Sato, H. Shinohara, and N. Nishi, *Chem. Phys.*, **73**, 377 (1982).
10) M. Kawasaki and H. Sato, *Chem. Phys. Lett.*, **139**, 585 (1987).
11) H. Kanamori, J. E. Butler, K. Kawaguchi, C. Yamada, and E. Hirota, *J. Chem. Phys.*, **83**, 611 (1985).
12) T. Ebata, O. Nakazawa, and M. Ito, *Chem. Phys. Lett.*, **143**, 31 (1988).
13) P. Felder, C. S. Effenhauser, B. M. Haas, and J. R. Huber, *Chem. Phys. Lett.*, **148**, 417 (1988).
14) T. H. Dunning, Jr., *J. Chem. Phys.*, **53**, 2823 (1970).
15) S. Huzinaga, *J. Chem. Phys.*, **42**, 1293 (1965).
16) H. F. Schaefer, III, "Methods of Electronic Structure Theory," Plenum, New York (1977).
17) S. Huzinaga, *J. Chem. Phys.*, **53**, 451 (1970).
18) W. J. Hunt and W. A. Goddard, III, *Chem. Phys. Lett.*, **3**, 414 (1969).
19) J. C. D. Brand, P. H. Chiu, A. R. Hoy, and H. D. Bist, *J. Mol. Spectrosc.*, **60**, 43 (1976); A. R. Hoy and J. C. D. Brand, *Mol. Phys.*, **36**, 1409 (1978).
20) G. Herzberg, "Electronic Spectra and Electronic Structure of Polyatomic Molecules," Van Nostrand, Princeton (1969).
21) P. J. Hay, T. H. Dunning, Jr., and W. A. Goddard, III, *J. Chem. Phys.*, **62**, 3912 (1975); **67**, 2290 (1977).
22) L. E. Brus and J. R. McDonald, *J. Chem. Phys.*, **61**, 97 (1974).
23) P. J. Hay, R. T. Pack, R. B. Walker, and E. J. Heller, *J. Phys. Chem.*, **86**, 862 (1982).
24) D. Imre, J. L. Kinsey, A. Sinha, and J. Krenos, *J. Phys. Chem.*, **86**, 5027 (1982).
25) R. Vasudev and W. M. McClain, *J. Mol. Spectrosc.*, **89**, 125 (1981).
26) MELD: E. R. Davidson, L. E. McMurchie, S. T. Elbert, S. R. Langhoff, D. Rawlings, and D. Feller (Quantum Chemistry Group, University of Washington), IMS Computer Center, Library Program No. 030.